High frequency sky wave propagation during geomagnetic field reversals

MARIANO FAGRE[1,2], BRUNO S. ZOSSI[3,4], ERDAL YIĞIT[5], HAGAY AMIT[6] AND ANA G. ELIAS[3,4]✉

1 Consejo Nacional de Investigaciones Científicas y Técnicas, CONICET, Argentina

2 Laboratorio de Telecomunicaciones, Dpto. de Electricidad, Electrónica y Computación, Facultad de Ciencias Exactas y Tecnología, Universidad Nacional de Tucuman, Argentina

3 Laboratorio de Física de la Atmosfera, Dpto. de Física, Facultad de Ciencias Exactas y Tecnología, Universidad Nacional de Tucuman, Argentina (aelias@herrera.unt.edu.ar)

4 INFINOA (CONICET-UNT), Tucuman, Argentina

5 Space Weather Laboratory, Department of Physics and Astronomy, George Mason University, USA

6 CNRS, Université de Nantes, Nantes Atlantiques Universités, Laboratoire de Planétologie et de Géodynamique, Nantes, France

Received: July 16, 2019; Revised: November 13, 2019; Accepted: November 18, 2019

ABSTRACT

The ionosphere, a plasma embedded in the Earth's magnetic field, affects propagation of electromagnetic waves in the high frequency range since the refractive index at these frequencies depends on a combination of plasma density and magnetic field intensity and direction. In particular, the ground range of high frequency waves that reflect in the ionosphere, or sky waves, presents detectable Earth's magnetic field effects. This field varies greatly, with the most drastic scenario being a polarity reversal. The spatial variability of the ground range during possible reversal scenarios is analyzed in the present work using numerical ray tracing. In order to isolate the magnetic field effect we exclude the effect of changing ionospheric conditions by considering a uniform ionosphere. Our results show that the ground range increases with increasing ray alignment with the field direction as well as with increasing magnetic field intensity. For the present field that is dominated by an axial dipole, the ground range is greatest for northward propagation at the magnetic equator. A similar situation occurs for a prevailing equatorial dipole with eastward propagation at the corresponding magnetic equator that here runs almost perpendicular to the geographic equator. For less dipolar configurations the ground range spatial variability becomes smaller. Although a reversal is foreseeable only in a very distant future, studying potential consequences during a reversal may highlight possible effects of dipole decrease which is already ongoing at present. In addition to the geophysical insight, our results may have applications for communication and radar systems.

Keywords: ray tracing, radiowave propagation, Earth's magnetic field, paleomagnetism

Stud. Geophys. Geod., 64 (2020), 130–142, DOI: 10.1007/s11200-019-1154-2

1. INTRODUCTION

Radio frequency electromagnetic waves between 3 and 30 MHz, designated as high-frequency (HF) waves by the International Telecommunication Union (ITU), are used in long-distance communications and detection, and have been of interest since the 1920's for practical reasons. Since the advent of telecommunication systems it has been a challenge to establish radio links as well as exact positions with radar systems using the ionosphere as a reflector due to the theoretical complexity of electromagnetic wave propagation through the ionospheric plasma that is embedded in the Earth's magnetic field. To solve this problem and to estimate the ray path between the transmitter and a long-range target, the ray tracing technique is commonly employed. Different methods have been developed, motivated by the fast progress in computational resources (*Settimi and Bianchi, 2014*).

Ray tracing is a powerful and useful tool that allows determining the exact path of radio waves given a precise knowledge of the refractive index along the propagation path. To include a realistic ionosphere and geomagnetic field, ray tracing must be assessed numerically in order to obtain desired outputs, such as a sky wave ground range and reflection height. A numerical ray tracing technique that has been widely used is that of *Jones and Stephenson (1975)*, which calculates ray paths and associated quantities in three-dimensional space.

A key parameter in ray tracing is the ionospheric refractive index, which depends primarily on electron density and to a much lesser extent on the magnetic field intensity and orientation (*Davies, 1965*). The ionosphere is a medium with high space-time variability in electron concentration, even under geomagnetic quiet conditions. Ionization processes strongly depend on solar radiation, which in turn depends on solar zenith angle, that is local time, season and location, and also on solar activity level. However, in order to isolate the magnetic field effect in the present work we exclude the effect of changing ionospheric conditions by considering a uniform ionosphere. If we consider a more realistic ionosphere, as that given by the International Reference Ionosphere model (IRI) (e.g., *Bilitza, 2018*), the most noticeable effect would be the latitudinal variation of the electron density. The most pronounced variation appears at the F2 peak height due to the equatorial ionization anomaly that is a partially depleted region above the magnetic equator, and two enhanced regions at both of its sides at latitude of ~15°. To this, the natural latitudinal gradient due to the season in turn should be added. These electron density variations produce stronger variations in ray tracing than the Earth's magnetic field. Thus the natural ionization variation should be filtered out in order to isolate the geomagnetic effect. This filtering is almost equivalent to considering a uniform ionosphere. There is in addition, the effect over the ionosphere itself of the Earth's magnetic field variations, which we are not considering, since we are presenting in this work a first approximation to the problem without feedback.

The present field can be approximated by a geocentric magnetic dipole with its axis tilted about 11° with respect to Earth rotational axis. This dipole accounts for ~80% of the magnetic field power at Earth's surface (*Merrill et al., 1998*), while the remaining ~20% is made up by non-dipolar components. Paleomagnetic measurements show that Earth's magnetic field varies greatly, with the most dramatic changes being polarity reversals that

take place on average every ~200000 years (*Jacobs, 1994*; *Glassmeier et al., 2009*). However, the time period of same polarity between reversals (termed chron) can be highly variable, ranging tens thousands to tens millions of years (*Olson and Amit, 2015*), with the last reversal occurring about 780000 years ago (*Jacobs, 1994*).

The duration of a polarity reversal is a few thousand years (*Clement, 2004*). During this period the field magnitude at the Earth surface may diminish to about 10% of its normal value. Although the understanding of geomagnetic reversals has improved considerably over the years with paleomagnetic data acquisitions and numerical geodynamo simulations (*Valet and Fournier, 2016*), detailed reversal properties, in particular the evolution of the multi-polar part of the field during a polarity transition, are still under debate. Obviously the axial dipole vanishes during a reversal when the dipole axis crosses the equator. *Amit et al. (2010)* summarized several reversal scenarios with two extremes for the dipolar component: a dipole collapse and a dipole rotation from one hemisphere to the other. In the latter case, only the axial dipole would vanish by transferring its energy to the equatorial dipole components. Regarding the non-dipolar field, *Amit et al. (2010)* considered three main possibilities: (1) decrease in phase with the dipole collapse, (2) remains unchanged, or (3) grows throughout the reversal possibly due to energy transfer from the dipole (*Amit and Olson, 2010*; *Huguet and Amit, 2012*), or dynamo configurations favouring the generation of a non-dipolar field.

Variations in Earth's magnetic field (strength and morphology) can impact HF wave propagation, thermosphere-ionosphere dynamics, and manifestation of space weather. Although numerous works analysed ray tracing results considering the geomagnetic field effect (*Milington, 1951*; *Rao, 1969*; *Tsai et al., 2010*; *Dao et al., 2016*), the consequences of the field's secular variation on HF wave propagation with a paleomagnetic perspective has not been thoroughly studied yet. This is an interesting topic from a geophysical point of view in addition to its potential applications in communication and radar systems. Although a reversal is foreseeable only in a very distant future, studying ionospheric dynamics during a reversal may highlight possible effects of dipole decrease which is already ongoing at present (e.g., *Olson and Amit, 2006*; *Finlay, 2008*; *Finlay et al., 2016*; *Huguet et al., 2018*).

In the present work the global spatial variability of the ground range is determined for three different geomagnetic field configurations during reversals: an axial dipole collapse, a dipole rotation, and an energy cascade. These scenarios were recently considered to study the effects of paleomagnetic reversals on the ionosphere, including the ionospheric Hall and Pedersen conductances (*Zossi et al., 2018*) as well as the polar caps (*Zossi et al., 2019*). In Section 2 we outline the theoretical background of our study, followed by the methodology in Section 3. Results are presented in Section 4 followed by discussion in Section 5.

2. THEORY

The Earth's magnetic field turns the ionosphere into an anisotropic medium, producing three main effects on the refraction of an incident electromagnetic wave: (i) double refraction, (ii) the direction of energy flow differs from that of the wave propagation, and (iii) the refractive index, n, depends on the angle of refraction hindering the solution of

Snell's law directly. Regarding the first effect, the ionosphere, as any magnetized plasma, becomes a doubly refracting medium decomposing an incident linearly polarized wave into two modes of propagation for which the terms "ordinary" and "extraordinary" are taken from crystal optics, with subscripts "o" and "x" denoting each mode respectively. We will consider the ordinary ray mode, which is visible most of the time. The second effect turns asymmetrical the ray path of an oblique propagating electromagnetic signal with respect to the reflection point, and deviates the path laterally out of the plane of incidence. Regarding the third effect, assuming a cold magnetoplasma where only electrons need to be taken into account (valid approximation for the propagation of HF signals in the ionosphere), n can be estimated from the Appleton-Hartree equation (*Davies, 1965*), that is,

$$n = \sqrt{1 - \frac{2X(1-X)}{2(1-X) - Y_T^2 \pm \sqrt{Y_T^2 + 4(1-X)^2 Y_L^2}}}, \tag{1}$$

with

$$X = \frac{f_o^2}{f^2} = \frac{Ne^2}{m\varepsilon_0 (2\pi f)^2}, \tag{2}$$

$$Y_T = Y \sin\Theta = \frac{eB}{m(2\pi f)} \sin\Theta, \tag{3}$$

$$Y_L = Y \cos\Theta = \frac{eB}{m(2\pi f)} \cos\Theta, \tag{4}$$

$$Y = \frac{eB}{m(2\pi f)}, \tag{5}$$

where f_o is the plasma frequency, f the incident electromagnetic wave frequency, N the electron number density, e the electron charge, m the electron mass, ε_0 the vacuum permittivity, B the magnetic field intensity, T stands for transverse and L for longitudinal, and Θ is the angle between the direction of the wave propagation and the magnetic field vector. The upper sign in the denominator of Eq. (1) refers to the ordinary component and the lower sign to the extraordinary angle Θ, which varies along the ray path in the ionosphere, is given by

$$\cos\Theta = \cos I \cos\alpha (\cos D \cos\gamma + \sin D \sin\gamma) + \sin I \sin\alpha, \tag{6}$$

where D and I are the geomagnetic field declination and inclination, respectively, α the elevation angle of the electromagnetic signal emitted by the transmitter, and γ the direction of the ray path, that is 0° and 90° for northward and eastward propagation respectively.

The next step is to determine the ray path using ray tracing. Since Snell's law calculations are practical only in isotropic conditions and when the ray path is confined to two dimensions, which is not our case, we determine the ray path based on Hamilton's

equations. The ground range is finally obtained from the ray path as the measure of the distance along Earth's surface from the ray's origin (a transmitter) to the point where it again reaches Earth's surface (a receiver or a target).

3. METHODOLOGY

3.1. Earth's magnetic field configurations

The International Geomagnetic Reference Field 12-th Generation (IGRF-12) (*Thébault et al., 2015*) was used to specify the pre-reversal magnetic field for three plausible reversal scenarios: an axial dipole collapse where the axial dipolar component is set to zero while maintaining the equatorial dipole components as well as higher degrees unchanged, a dipole rotation where the power of the axial dipole component is transferred to the equatorial dipole components proportional to their pre-reversal powers, and an energy cascade where the power of the dipolar components is transferred to the quadrupolar and octupolar components. For the last two scenarios, a constant total magnetic power on the core-mantle boundary calculated based on the Mauersberger-Lowes spectrum (*Lowes, 1974*) was considered. These scenarios, and the way we calculated the corresponding Gauss coefficients at the heights of the reversal scenarios are described in detail in *Zossi et al. (2019)*.

3.2. HF signal ray tracing procedure

Various numerical ray tracing programs have been developed. Among them, *Azzarone et al. (2012)* developed a software that is freely available and allows ionospheric ray tracing in a geocentric spherical coordinate system, taking into account a dipolar geomagnetic field. However, since we consider multi-harmonic fields, the 3D ray tracing original code developed by *Jones and Stephenson (1975)* was adjusted to take as inputs the IGRF-12 model and the configurations for the transitional magnetic field. This ray tracing is based on Hamilton's equations of geometrical optics given by *Haselgrove (1955)* in spherical coordinates. The software to obtain the ray path and the integration algorithm are from the Fortran code by *Jones and Stephenson (1975)*, including the improvements and corrections made by *Azzarone et al. (2018)*.

3.3. Calculation setup

The global spatial structure of ground range for an oblique propagation is assessed on a grid with 5° latitude and 10° longitude resolution with which we obtain well defined patterns, adequate for Earth's surface magnetic field even under a field reversal with a dominant multipolar configuration, with the least calculations. The resolution is higher for latitude because the ionosphere is more variable in this component. At each grid point, ray tracing steps for each estimated ray path are less than a kilometer.

A single electron density height profile was used for the whole grid that consists in a β-Chapman layer. The plasma frequency f_o is then given by

$$f_o^2 = f_o \mathrm{F2}^2 \exp\left(1 - z - e^{-z}\right), \tag{7}$$

where

$$z = \frac{h - hm\mathrm{F2}}{H}, \tag{8}$$

and *hm*F2 is the peak height of the F2 layer. Typical f_oF2 and *hm*F2 values for 12 LT, quiet time and solar minimum conditions were considered, that is 8 MHz and 300 km, respectively. An isothermal ionosphere was considered with the typical 60 km value for the neutral scale height *H*, considering atomic oxygen as the main ionizable neutral component at the F2 region and a thermospheric neutral temperature around 1000 K at these heights typical of noon time and mid to low solar activity level at an average *hm*F2 ~300 km, as considered in this work. In general, above this height level the temperature gradient becomes much weaker than below, and usually from there an isothermal thermosphere can be assumed.

Northward and eastward wave propagation directions were considered with a fixed elevation angle $\alpha = 20°$, and a single frequency of 15 MHz, which are typical mean values for over-the-horizon radars, OTHR, which use Earth's ionosphere as a mirror to illuminate targets beyond the line-of-sight horizon.

4. RESULTS

Figure 1 shows the surface field intensity *B* obtained from the IGRF-12 model for present conditions and for the three reversal scenarios here considered. The axial dipole component is zero in the latter hence the intensity becomes less zonal and less axisymmetric in the three reversal scenarios than in the present field. The dipole rotation

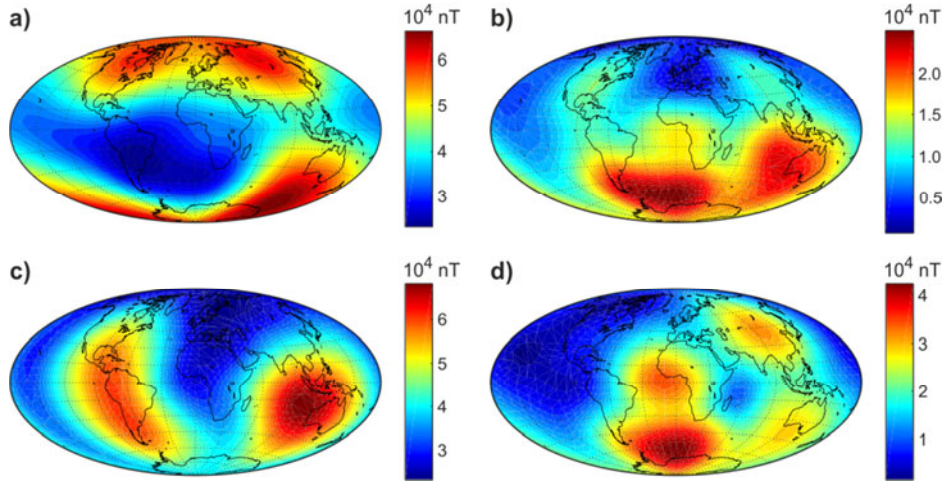

Fig. 1. Earth's surface magnetic field intensity *B*, obtained from IGRF-12 model for: **a)** present conditions, **b)** axial dipole collapse, **c)** rotation where axial dipole energy is transferred to the equatorial dipole, and **d)** energy cascade where dipolar energy is transferred to the quadrupolar and octupolar terms. Note the different scales for intensity.

scenario results in a dominant equatorial dipole (Fig. 1c), whereas the energy cascade scenario (Fig. 1d) resembles axial dipole collapse (Fig. 1b) but the former is characterized by smaller spatial scales.

Figures 2 and 3 present the corresponding ground range distributions for northward and eastward wave directions. Ray path, and hence the resulting ground range, are uniquely determined by the refractive index n. This index varies in a non-trivial way with the field intensity B and the ray-field angle Θ that depends on α, γ, I and D, as can be seen

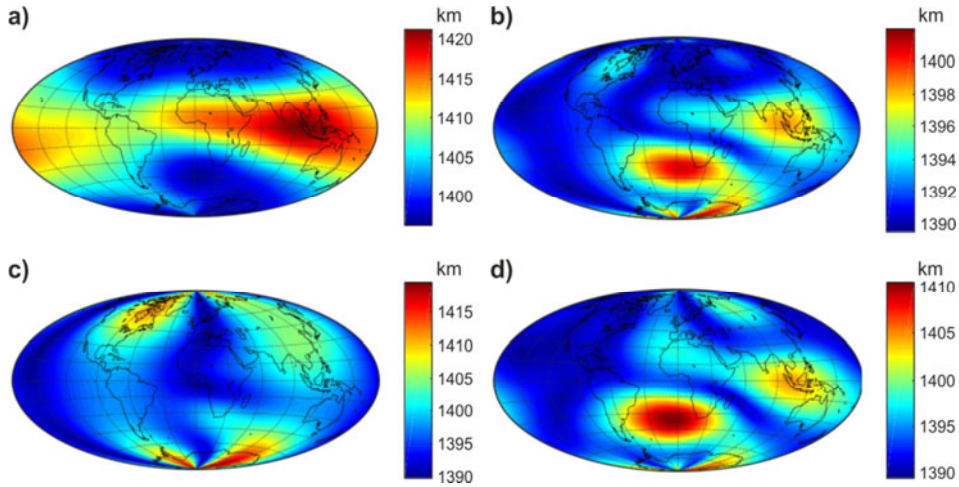

Fig. 2. Ground range for a northward propagating high-frequency wave of 15 MHz and a 20° elevation angle for the four field configurations shown in Fig. 1. Note the different scales.

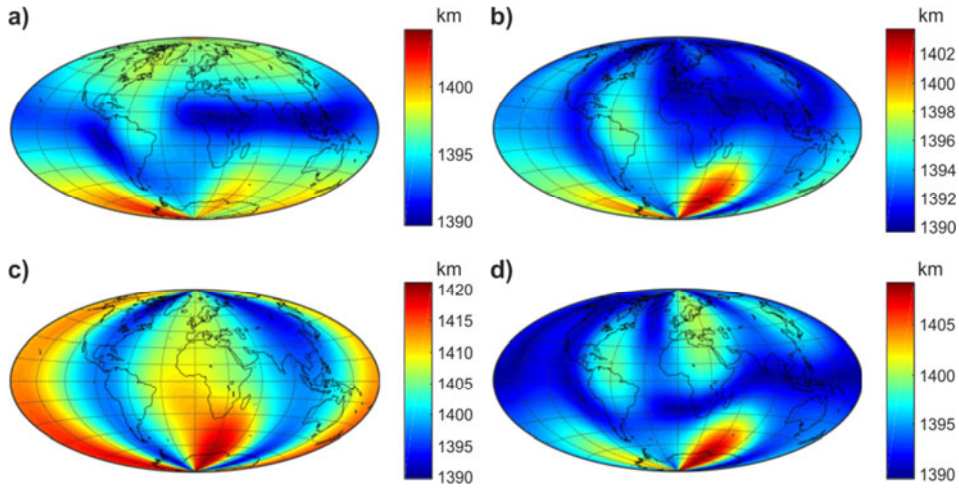

Fig. 3. The same as in Fig. 2 for an eastward propagating high-frequency wave.

in Eq. (6). Therefore, the relation between the field configuration and the resulting ground ranges is not straightforward. According to Eq. (1) n is closer to its free space value for increasing B and/or for lower Θ, i.e. for ray paths aligned with the field, with higher sensitivity to ray-field alignment for a given B, than to B for a given alignment.

To describe how the field configuration and its interaction with the wave propagation direction determine the ground range, consider the relations among the present day field intensity (Fig. 1a), the resulting ground ranges for northward (Fig. 2a) and eastward (Fig. 3a) propagations, and the field-wave angle at the ray origin, which is shown in Fig. 4a,b. The present day field is most aligned with the northward wave along the magnetic equator (Fig. 4a), leading to the greatest ground range values there (Fig. 2a) even though in this region the field intensity is lowest (Fig. 1a). The ground range is largest in Indonesia (Fig. 2a) where the intensity is least low in the equatorial belt (Fig. 1a). In the case of eastward propagation the greatest alignment occurs in the South Pacific (Fig. 4b) where the intensity is also high (Fig. 1a), hence the ground range for eastward propagation is largest there with maximum $R \sim 1400$ km (Fig. 3a). However, the largest values for northward propagation are larger with maximum $R \sim 1420$ km, because the ray-field alignment degree is higher in the northward propagation case (maximum eastward alignment: $\cos\Theta = 0.609$, that is $\Theta \sim 52°$, versus maximum northward alignment: $\cos\Theta = 1$, that is $\Theta \sim 0°$, that is perfect alignment).

The axial dipole collapse case presents the weakest B values (Fig. 1) but comparison of Fig. 2b,d and Fig. 3b,d reveals that its ground range spatial patterns are similar to those of the energy cascade case (for which B is almost double), due to a similar field morphology as expressed by the inclination and declination (*Zossi et al., 2019*). In both cases, for the northward wave the ground range is largest in an east-west strip in the south Atlantic (Fig. 2b,d) where both the intensity (Fig. 1b,d) and the field alignment (Fig. 4c,g) are large. Similarly, for the eastward wave the ground range is largest in a north-south strip in the Indian Ocean (Fig. 3b,d) where again both the intensity (Fig. 1b,d) and the field alignment (Fig. 4d,h) are large.

In the dipole rotation scenario, the field is most aligned with the eastward wave at the corresponding magnetic Equator which runs along the meridian through Africa and mid-Pacific (Fig. 4f). It somewhat resembles the present magnetic field case, in the sense that, since the field corresponds almost to a 90° rotation, the eastward ground range spatial pattern (Fig. 3c) is similar to the northward case for the present field (Fig. 2a).

Overall, a rather good agreement between the wave to field lines alignment and the ground range in the different magnetic field scenarios can be noticed. However, due to the additional dependence on the field intensity, some discrepancies exist. For example, in the energy cascade scenario the ray-field alignments are characterized by numerous small scale features (Fig. 4g,h) whereas the maximal ground ranges are localized at single locations (Figs 2d and 3d) where overlaps with high intensity structures prevail (Fig. 1d).

5. DISCUSSION

In the absence of a magnetic field, for the ray tracing conditions considered here, we would obtain a uniform ground range distance of 1390 km for both propagation directions (northward and eastward) for the whole globe. With the present magnetic field, the ground

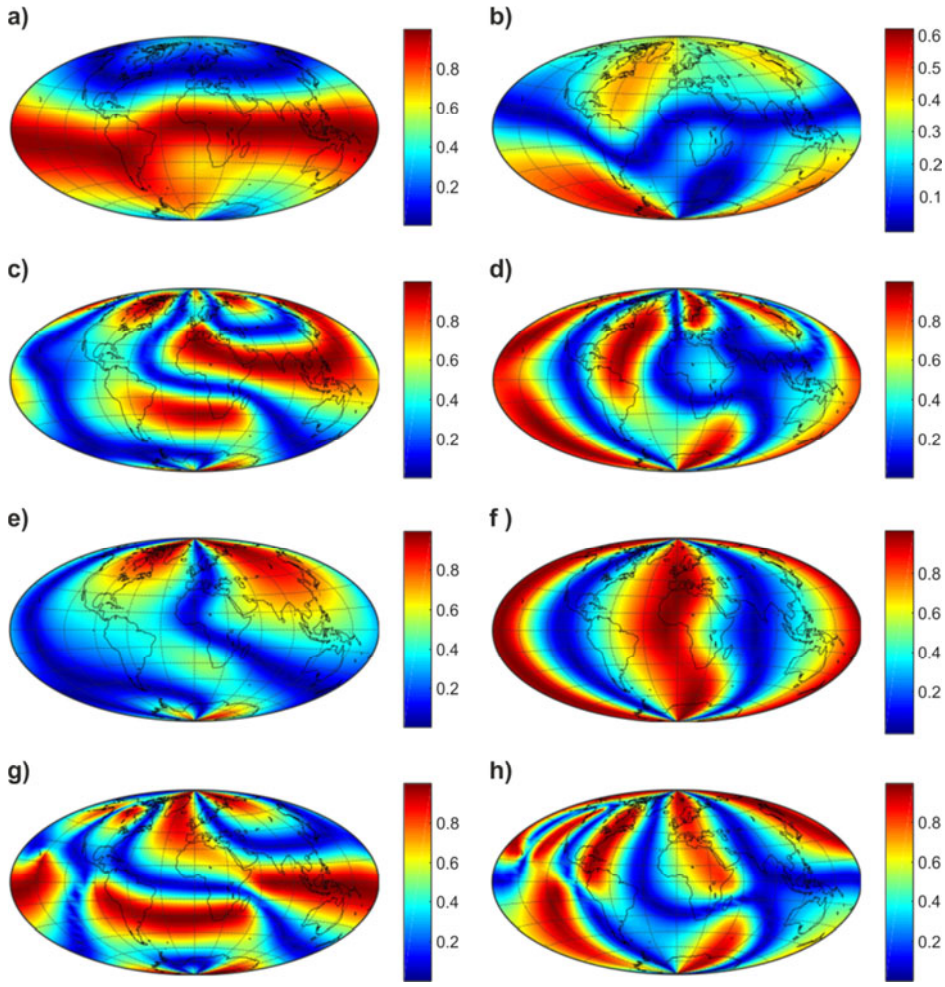

Fig. 4. Cosine of angle Θ between the incident high-frequency wave at the base of the ionosphere and the Earth's magnetic field direction for: **a)** and **b)** the present Earth's magnetic field; **c)** and **d)** axial dipole collapse; **e)** and **f)** a dipole rotation; and **g)** and **h)** an energy cascade. Left panels correspond to northward and right panels to eastward propagation.

range is no longer uniform, varying between ~1390 and ~1420 km for northward propagation and between ~1390 and ~1400 km for eastward propagation. These extreme values differ very little among the considered field scenarios, by at most 2%. The main variation in the global pattern is related to the cos Θ value, which in turn depends on the ray direction, and the field inclination and declination global distributions. In addition, the ground range depends on the field intensity in a non-trivial way.

Inside Earth's outer core, the alignment of the fluid flow and the magnetic field determines the efficiency of induction. In particular, at the top of the core horizontal flow

that is parallel to radial field isolines produces zero advective secular variation, which is a severe inherent problem for inferring the flow from geomagnetic observations (e.g., *Backus and Bullard, 1968*). Non-linear magnetohydrodynamic effects tend to align the flow and the field hence to minimize their interaction (*Aubert, 2005*; *Cao et al., 2018*). At the top of the core, numerical dynamos exhibit large alignment at high-latitude intense flux patches which are correlated with axial columnar cyclones that maintain these features, whereas low-latitude drifting field structures are advected by a flow that is nearly perpendicular to these patches (*Finlay and Amit, 2011*). This bimodal behavior gives an intermediate value for the globally averaged alignment (*Finaly and Amit, 2011*; *Peña et al., 2016*). Overall, understanding the flow-field alignment in the core is crucial for properly inferring core dynamics just as accounting for wave-field alignment in the ionosphere reveals the spatial variability of ground range.

The greatest difference between ground range values for the present field and the reversal scenarios considered here is around 30 km. Even though small in percentage terms, these values could matter for certain applications, such as higher order ionospheric effects for trans-ionospheric propagation that are increasingly relevant as precision requirements on Global Positioning System (GPS) data and products increase. In this respect, the ionosphere is a significant error source for Global Navigation Satellite Systems (GNSS) and GPS data. These errors may vary from a few centimeters to tens of meters. Most of it can be corrected by combining signals at two frequencies. However, higher order errors remain, such as the second order ionospheric term in the refractive index formula which depends precisely on the geomagnetic field. These errors become some of the main limiting factors for applications where millimeter level accuracy is demanded (*Hoque and Jakowski, 2008*; *Petrie et al. 2011*). The dipole model, which is a cruder representation of Earth's geomagnetic field than the true multi harmonic field, is sometimes used. However, even though the resulting coordinate differences are not large, considering the true field is crucial (*Petrie et al., 2011*), since the difference in the second order error between the dipole and the full IGRF model can be up to 60%, mainly in the South Atlantic Anomaly (*Hernández-Pajares et al., 2007*). In a different kind of analysis, *Dao et al. (2016)* found that Earth's magnetic field effects can limit the accuracy of the mirror model (MM) used for geolocation.

A strong assumption we made is that the ionosphere will be during the reversal scenarios as it is now. Earth's magnetic field affects electron density variability essentially at the F2 layer from the peak upwards. The lower layers of the ionosphere, i.e. the E and F1 regions, are mainly under a photo-chemical regime, so changes in the solar radiation and solar zenith angle are expected to be the dominant variation sources. In the F2 layer, plasma diffusion becomes important and the magnetic field reduces the effectiveness of diffusion due to ions and electrons which are forced to diffuse exclusively along magnetic field lines at these heights. Changes in the magnetic field inclination and declination then can move up and down the F2 peak height thus affecting the ionization density. Energetic particle precipitation, which is also a source of ionization, would present stronger changes with the magnetic field variations. However, we emphasize that it is a source of transient character and can be considered as filtered out by the time scale here considered as in the case of high frequency ionization variations. *Cnossen et al. (2011)* estimated for a 25% reduction in the dipole moment of the Earth an increase in temperature, causing the thermosphere to expand and ionospheric layers to move upwards, since these layers tend

to stay on constant pressure surfaces. They found that the electron density is more affected at equinox with a ~10% variation, while there is little difference at solstice. Even though we examine stronger decreases in the magnetic field, we still consider valid our assumption of a constant ionosphere as a first approximation. We are assuming in this case that solar radiation and solar wind will have the same characteristics during reversals as today.

The significantly larger amplitude sources of ionization variation are of much shorter timescales (from seconds up to decades) than the geomagnetic timescale here considered of several thousand years (typical duration of a field transition). For long-term processes such as reversals high frequency electron density variations are thus completely averaged out, hence the lack of their consideration in our models. This time scale separation is analogous to global warming in the troposphere that corresponds to a long-term (low frequency) increase of tenths of a degree compared to the ~20–30 or even more degrees of much higher frequency variability if one considers diurnal or seasonal temperature variations (*IPCC, 2014*). Another relevant example is core-mantle interactions on time scales of Myrs. In this case the very long-term time-average paleomagnetic field over the past 5 Myrs is considered, which is characterized by much weaker spatial variability than the instantaneous field, but it serves to isolate the persistent effect of mantle control on the geodynamo (e.g., *Amit et al., 2015*).

Although a reversal is foreseeable in a very distant future, studying potential consequences during a reversal may highlight possible effects of dipole decrease which is already ongoing at present. Overall, the study of geomagnetic field and secular variation effects on electromagnetic wave propagation through the ionospheric plasma is an interesting topic from a geophysical point of view and also for its potential applications in communication and radar systems.

Acknowledgements: We thank Anna Belehaki for constructive comments that improved the paper.

References

Amit H. and Olson P., 2010. A dynamo cascade interpretation of the geomagnetic dipole decrease. *Geophys. J. Int.*, **181**, 1411–1427.

Amit H., Leonhardt R. and Wicht J., 2010. Polarity reversals from paleomagnetic observations and numerical dynamos simulations. *Space Sci. Rev.*, **155**, 293–335.

Amit H., Choblet G., Olson P., Monteux J., Deschamps F., Langlais B. and Tobie G., 2015. Towards more realistic core-mantle boundary heat flux patterns: a source of diversity in planetary dynamos. *Prog. Earth Planet. Sci.*, **2**, 22–26.

Aubert J., 2005. Steady zonal flows in spherical shell fluid dynamos. *J. Fluid Mech.*, **542**, 53–67.

Azzarone A., Bianchi C., Pezzopane M., Pietrella M., Scotto C. and Settimi, A., 2012. IONORT: A Windows software tool to calculate the HF ray tracing in the ionosphere. *Comput. Geosci.*, **42**, 57–63.

Backus G.E. and Bullard C., 1968. Kinematics of geomagnetic secular variation in a perfectly conducting core. *Philos. Trans. R. Soc. A-Math. Phys. Eng. Sci.*, **263**, 239–266.

Bilitza D., 2018. IRI the international standard for the ionosphere. *Adv. Radio Sci.*, **16**, 1–11.

Cao H., Yadav R.K. and Aurnou J.M., 2018. Geomagnetic polar minima do not arise from steady meridional circulation. *Proc. Nat. Acad. Sci. USA*, **115,** 11186–11191.

Clement B.M., 2004. Dependence of the duration of geomagnetic polarity reversals on site latitude. *Nature*, **428**, 637–640.

Cnossen I., Richmond A.D., Wiltberger M., Wang W. and Schmitt P., 2011. The response of the coupled magnetosphere-ionosphere-thermosphere system to a 25% reduction in the dipole moment of the Earth's magnetic field. *J. Geophys Res.-Space Phys.*, **116**, A12304.

Dao E.V., McNamara L.F. and Colman J.J., 2016. Magnetic field effects on the accuracy of ionospheric mirror models for geolocation. *Radio Sci.*, **51**, 284–300.

Davies K., 1965. *Ionospheric Radio Propagation*. National Bureau of Standards Monograph **80**. U.S. Dept. of Commerce, Washington, D.C.

Finlay C.C., 2008. Historical variation of the geomagnetic axial dipole. *Phys. Earth Planet. Inter.*, **170**, 1-14.

Finlay C.C. and Amit H., 2011. On flow magnitude and field-flow alignment at Earth's core surface. *Geophys. J Int.*, **186**, 175–192.

Finlay C.C., Aubert J. and Gillet N., 2016. Gyre-driven decay of the Earth's magnetic dipole. *Nat. Commun.*, **7**, 10422.

Glassmeier K.H., Soffel H. and Negendank J.F.W., 2009. *Geomagnetic Field Variations*. Springer Verlag, Berlin, Germany.

Haselgrove J., 1955. Ray theory and a new method for ray tracing. *Physics of the Ionosphere*. The Physical Society, London, U.K., 355–364.

Hernández-Pajares M., Juan J.M., Sanz J. and Orús R., 2007. Second-order ionospheric term in GPS: Implementation and impact on geodetic estimates. *J. Geophys Res.-Solid Earth*, **112**, B08417.

Hoque M.M. and Jakowski N., 2008. Estimate of higher order ionospheric errors in GNSS positioning. *Radio Sci.*, **43**, RS5008.

Huguet L. and Amit H**., 2012.** Magnetic energy transfer at the top of Earth's core. *Geophys. J. Int.*, **190**, 856–870.

Huguet L., Amit H. and Alboussière T., 2018. Geomagnetic dipole changes and upwelling/downwelling at the top of the Earth's core. *Front. Earth Sci.*, **6**, UNSP 170.

IPCC, 2014. *Climate Change 2014. Synthesis Report.* Contribution of Working Groups I, II and III to the Fifth Assessment Report of the Intergovernmental Panel on Climate Change. IPCC, Geneva, Switzerland.

Jacobs J.A., 1994. *Reversals of the Earth's Magnetic Field*. Cambridge University Press, Cambridge, U.K.

Jones R.M. and Stephenson J.J., 1975. *A Versatile Three-Dimensional Ray Tracing Computer Program for Radio Waves in the Ionosphere*. Office of Telecommunications Report **75-76**. U.S. Department of Commerce, Washington, D.C.

Lowes F.J., 1974. Spatial power spectrum of the main geomagnetic field, and extrapolation to the core. *Geophys. J. R. Astron. Soc.*, **36**, 717–730.

Merrill R.T., McElhinny M.W. and McFadden P.L.,1998. *The Magnetic Field of the Earth*. Academic Press, San Diego, CA.

Millington G., 1951. The effect of the Earth's magnetic field on short-wave communication by the ionosphere. *Proc. IEE - Part III: Radio Commun. Eng.*, **98**, 314–319, DOI: 10.1049 /pi-3.1951.0064.

Olson P. and Amit H., 2006. Changes in Earth's dipole. *Naturwissenschaften*, **93**, 519–542.

Olson P. and Amit H., 2015. Mantle superplumes induce geomagnetic superchrons. *Front. Earth Sci.*, **3**, UNSP 38.

Peña D., Amit H. and Pinheiro K.J., 2016. Magnetic field stretching at the top of the shell of numerical dynamos. *Earth Planets Space*, **68**, 78.

Petrie E.J., Hernández-Pajares M., Spalla P., Moore P. and King M.A., 2011. A review of higher order ionospheric refraction effects on dual frequency GPS. *Surv. Geophys.*, **32**, 197–253.

Rao N.N., 1969. Bearing deviation in high-frequency transionospheric propagation: 3. Ray tracing investigation of the magnetoionic effect. *Radio Sci.*, **4**, 153–161.

Settimi A. and Bianchi S., 2014. Ray theory formulation and ray tracing method. Application in ionospheric propagation. *Quaderni di Geofisica*, N°121, Istituto Nazionale di Geofisica e Vulcanologia (INGV), Rome, Italy.

Thébault E., Finlay C.C., Beggan C., Alken P., Aubert J., et al., 2015. International Geomagnetic Reference Field: the 12th generation. *Earth Planets Space*, **67**, 79.

Tsai L.C., Liu C.H. and Huang J.Y., 2010. Three-dimensional numerical ray tracing on a phenomenological ionospheric model. *Radio Sci.*, **45**, RS5017.

Valet J.P. and Fournier A., 2016. Deciphering records of geomagnetic reversals. *Rev. Geophys.*, **54**, 410–446.

Zossi B.S., Elias A.G. and Fagre M., 2018. Ionospheric conductance spatial distribution during geomagnetic field reversals. *J. Geophys Res.-Space Phys.*, **123**, 2379–2397.

Zossi B.S., Fagre M., Amit H. and Elias A.G., 2019. Polar caps during geomagnetic polarity reversals. *Geophys. J. Int.*, **216**, 1334–1343.